

# Possibilities and challenges when using synthetic computed tomography in an adaptive carbon-ion treatment workflow

Barbara Knäusl <sup>a,b,\*</sup>, Peter Kuess <sup>a,b</sup>, Markus Stock <sup>b</sup>, Dietmar Georg <sup>a</sup>, Piero Fossati <sup>b</sup>, Petra Georg <sup>b</sup>, Lukas Zimmermann <sup>a,c,d</sup>

<sup>a</sup> Medical University of Vienna, Department of Radiation Oncology, Währinger Gürtel 18–20, 1090 Vienna, Austria

<sup>b</sup> MedAustron Ion Therapy Center, Wiener Neustadt, Marie-Curie-Straße 5, 2700 Wiener Neustadt, Austria

<sup>c</sup> Faculty of Health, University of Applied Sciences Wiener Neustadt, Johannes-Gutenberg-Straße 3, 2700 Wiener Neustadt, Austria

<sup>d</sup> Competence Center for Preclinical Imaging and Biomedical Engineering, University of Applied Sciences Wiener Neustadt, Johannes-Gutenberg-Straße 3, 2700 Wiener Neustadt, Austria

Received 16 March 2022; accepted 29 May 2022

## Abstract

**Background and purpose:** Anatomical surveillance during ion-beam therapy is the basis for an effective tumor treatment and optimal organ at risk (OAR) sparing. Synthetic computed tomography (sCT) based on magnetic resonance imaging (MRI) can replace the X-ray based planning CT (X-rayCT) in photon radiotherapy and improve the workflow efficiency without additional imaging dose. The extension to carbon-ion radiotherapy is highly challenging: complex patient positioning, unique anatomical situations, distinct horizontal and vertical beam incidence directions, and limited training data are only few problems. This study gives insight into the possibilities and challenges of using sCTs in carbon-ion therapy.

**Materials and methods:** For head and neck patients immobilised with thermoplastic masks 30 clinically applied actively scanned carbon-ion treatment plans on 15 CTs comprising 60 beams were analyzed. Those treatment plans were recalculated on MRI based sCTs which were created employing a 3D U-Net. Dose differences and carbon-ion spot displacements between sCT and X-rayCT were evaluated on a patient specific basis.

**Results:** Spot displacement analysis showed a peak displacement by 0.2 cm caused by the immobilisation mask not measurable with the MRI. 95.7% of all spot displacements were located within 1 cm. For the clinical target volume (CTV) the median  $D_{50\%}$  agreed within  $-0.2\%$  ( $-1.3$  to  $1.4\%$ ), while the median  $D_{0.01\text{ cc}}$  differed up to  $4.2\%$  ( $-1.3$  to  $25.3\%$ ) comparing the dose distribution on the X-rayCT and the sCT. OAR deviations depended strongly on the position and the dose gradient. For three patients no deterioration of the OAR parameters was observed. Other patients showed large deteriorations, e.g. for one patient  $D_{2\%}$  of the chiasm differed by  $28.1\%$ .

**Conclusion:** The usage of sCTs opens several new questions, concluding that we are not ready yet for an MR-only workflow in carbon-ion therapy, as envisaged in photon therapy. Although omitting the X-rayCT seems unfavourable in the case of carbon-ion therapy, an sCT could be advantageous for monitoring, re-planning, and adaptation.

**Keywords:** Synthetic CT; MR based workflow; Adaptive carbon-ion therapy; Deep learning

\* Corresponding author: Barbara Knäusl, Medical University of Vienna, Department of Radiation Oncology, Währinger Gürtel 18–20, 1090 Vienna, Austria.

E-mail: [barbara.knaeusl@meduniwien.ac.at](mailto:barbara.knaeusl@meduniwien.ac.at) (B. Knäusl).

## 1 Introduction

Excellent dosimetric accuracy and precise dose delivery are the basis of high-precision ion-beam therapy. Detailed knowledge of the anatomy and subsequent changes require repeated imaging and surveillance during the entire treatment course [1]. Magnetic resonance imaging (MRI) and its image transformation into synthetic computed tomography (sCT) data seems to be the ideal concept for this purpose reducing the additional imaging dose and acquisition time to a minimum [2]. In advanced photon therapy centres magnetic resonance (MR)-only treatment concepts are already close to clinical routine, especially for the pelvic and head region [3–6], while the particle therapy world lacks behind [7,8]. The requirements for sCTs in proton therapy are outlined in a review by Hoffmann et al. [8], focusing on accuracy and generation speed. The latter becomes important for real-time MR guided dose delivery, a promising technique also for proton and carbon-ion therapy [9,10]. Hoffmann et al. clearly state the need for improved sCT conversions for proton therapy and imply that the generation of sCTs does not depend on the network architecture, but more on the input training data set itself. Some studies investigated proton dose calculation accuracy on sCTs with patients who actually received a photon treatment for a proof of concept [11–13]. However, such an approach neglects the more challenging situation for carbon-ion therapy with limited beam angles in the absence of a rotating gantry, a setting which necessitates a non-standardized and highly individual treatment planning process. Moreover, there is no study currently displayed in the literature investigating the potential benefit and pitfalls of sCTs for treatments using carbon ions. A dosimetric difference between proton and carbon-ion therapy when applying sCTs is expected due to different physical parameters like lateral scattering, the carbon-ion fragmentation tail, and the particle spectra. Beyond that, relative radiobiological effectiveness (RBE) modelling and linear energy transfer (LET) affect the dose distribution and need also to be considered [14–17].

In contrast to proton therapy centres, most carbon-ion treatment facilities are limited to horizontal and vertical beamlines. In the world, only two centres have a carbon-ion gantry, *i.e.* HIT in Germany and NIRS in Japan [18–21]. Due to the restricted beam directions, an individual patient immobilisation, as well as varying positions for one patient, are common in carbon-ion therapy to allow a variety of multiple beam entrance directions. Non-standardized patient positions including tilts (by up to 45 degrees) and hyperextensions (bending in superior direction) of the head aiming to minimize the beam path through normal tissue, as well as bite blocks are posing new challenges to the sCT training process and question the applicability of sCTs in a carbon-ion therapy workflow.

In the past, various methods for sCT generation have been proposed, ranging from atlas-based [22,23] to deep learning approaches [24,25], where the latter has become the driving force in recent times. In a prior study an MR sequence independent sCTs generator was used [26], that had a strong clinical focus and concentrated on the applicability (*e.g.* dose distribution in the tumour and organs at risk (OARs)) in contrast to studies optimising the conversion process.

This study is the first investigation describing the impact and pitfalls of sCTs used instead of regular X-ray based planning CTs (X-rayCTs) for patients who received carbon-ion treatment, outlining several challenges that occur while treating rare cases with unique anatomy and multiple patient immobilisations. While such cases are infrequently treated with photon therapy, they represent the majority of patients in carbon-ion therapy, emphasising the need for an in-depth investigation with respect to new workflow components, like the inclusion of sCTs. The evaluation is based on comparisons of the dose distributions and spot positions.

## 2 Material and methods

### 2.1 Patient data, image acquisition and sCT generation

11 patients with head and neck tumors (six with adenoid cystic carcinomas and 5 with other histologies) were included in the planning analysis (range of clinical target volume (CTV) size: 5–353 cm<sup>3</sup>). A 3 mm margin was added to the CTV for planning target volume (PTV) creation.

All patients were treated at the MedAustron Ion Therapy Center [27] (Wiener Neustadt, Austria) within the registry trial (trial number GS1-EK-4/350-2015). For the included patients, either the BoS headframe System (QFix, US) with 3.2 mm thick Klarity thermoplastic masks (Klarity Medical Products, US) or the HeadStep with the iFrame and the 2 mm thick iCast thermoplastic masks (Elekta, Sweden) were used. In the clinical standard workflow all patients received an X-rayCT for dose calculation and multiple MRI sequences for OARs and target delineation two weeks before treatment. Those pre-treatment images were used for all further investigations in this study. All CTs and MRIs were sequentially acquired in treatment position employing all immobilisation devices (thermoplastic masks, vacuum mattresses, mold care) on the same day reducing the anatomical changes to a minimum. The subsequent acquisition required a repositioning of the patient when switching the imaging device. CT acquisition was performed with a Big Bore CT (Philips, Netherlands) using a specific head protocol with a voltage of 120 kV, an exposure of 300 mAs and a slice thickness of 2 mm. MRI images were acquired using an Ingenia 3.0 Scanner (Philips, Netherlands).

All patients received at least a  $T_2$  weighted (T2) sequence and a  $T_1$  weighted sequence with contrast medium (CM) (Prohance, Bracco Imaging S.p.A, Milan, Italy) injection (T1CM). For this study, clinical T1CM based on a spoiled gradient echo with an echo and recovery time of 3.4 ms and 7.2 ms, respectively, served as input sequence for sCT generation. The MRI and X-rayCT were aligned with the clinically applied rigid registration implemented in the treatment planning system (TPS) RayStation 8.1.1.8 (RaySearch Laboratories, Sweden).

The pre-trained model used for the sCT conversion is a 3D U-Net including ResNet blocks between up and down-sampling layers as described in Zimmermann et al. [26]. The model was trained on meningioma patients treated with proton therapy at the same institute. Furthermore, the same MRI scanner and sequences were employed providing the best possible training data set for this study. Three clinically applied sequences ( $T_1$ ,  $T_2$ , T1CM) were included in the training process and to improve convergence a feature based loss was incorporated. As shown by Zimmermann et al. [26] all sequences performed comparable in the sCT creation process with a mean absolute error (MAE) of 82.9 Houndsfield unit (HU).

## 2.2 Carbon-ion treatment planning

Clinical carbon-ion treatment plans were created on the X-rayCT in the TPS RayStation 8.1.1.8 with a  $2\text{ mm}^3$  calculation grid (dose calculation algorithm PB v3.0) employing the LEM1 model for biological dose calculation [28]. The HU to stopping power calibration [29] curve commissioned for the clinical CT protocol for head imaging was used. Those plans were subsequently recalculated on the respective sCT employing the identical CT calibration curve. The prescribed dose ranged from 50 to 68.8Gy biologically-weighted dose, with a fraction dose ranging from 2 to 5 Gy. One patient was treated with a simultaneous integrated boost while for all other patients different target volumes were treated sequentially. Clinical goals for the target and OARs were provided by the medical doctors on an individual basis for each patient. Robust optimisation considering setup and range uncertainties was employed if necessary to assure OAR sparing, e.g. the brainstem or the optical system. The majority of treatment plans was composed of two beams. In case of more beam directions or a boost, additional treatment plans were created, resulting in 2–8 beam directions per patient. Due to the limitation of a horizontal and vertical beam line, the beam incidence directions were restricted to feasible couch rotations.

For four cases an additional immobilisation, namely a second X-rayCT with a deviating patient position, was necessary to increase the degrees of freedom for beam

angles for treating the initial or the boost target volume. The evaluation of these four additional X-rayCTs was handled independently and henceforth included in the analysis summing up to 15 X-rayCTs for the 11 patients. In total 30 treatment plans with 60 beams were analysed on these 15 X-rayCTs and recalculated on the respective sCTs. In this study, all results were normalised to the dose per fraction and the different treatment plans were evaluated separately.

## 2.3 Evaluation and statistics

The image conversion performance was evaluated based on the MAE of the whole patient outline, excluding immobilisation equipment. The Euclidean distance between each carbon-ion spot position in the treatment plan, *i.e.* coordinate of the beam position to deliver a defined amount of particles, on the X-rayCT and sCT was calculated and plotted as a histogram. Respective beam positions were identified using the DICOM RT plan information retrieved from the TPS. Displacements were given in beam direction where negative and positive distances were defined as under- and overshoots, respectively.

Dose volume histogram (DVH) parameters were extracted for the target volumes, *i.e.* PTV and CTV, as well as for selected OARs, *e.g.* brainstem, chiasm, cochlea left/right, opticus left/right. For evaluation DVH parameters, like dose-to-volume (*i.e.*  $D_{2\%}$  is the dose to 2% of the region of interest) or volume-to-dose (*e.g.*  $V_{95\%}$  is the volume of the region of interest receiving 95% of the dose) were included:  $D_{0.1cc}$  and  $D_{2\%}$  as a surrogate for the maximum dose, the mean dose  $D_{50\%}, D_{98\%}$  as a surrogate for the minimum dose, as well as  $V_{95\%}$  and the conformity index (CI) for target coverage representation [30,31], where the latter was defined as:

$$CI = \frac{(PI \times TV)}{TV_{Pl}^2} \quad (1)$$

with  $PI$  as the volume of the 95% isodose,  $TV$  as the total CTV or PTV volume and  $TV_{Pl}$  as the CTV or PTV subvolume encompassed by the 95% isodose on the respective image. For the evaluation of dose differences only OARs receiving more than 5% of the prescribed dose were considered.

The MAE was calculated including all created sCT images and reported including its standard deviation (SD). Reported spot displacements were averaged over all treatment plans and presented as mean values with the respective SD. For dose values and dosimetric indices the respective results were reported as median values including the range. This presentation was also chosen for the percentage deviations between X-rayCT and sCT.

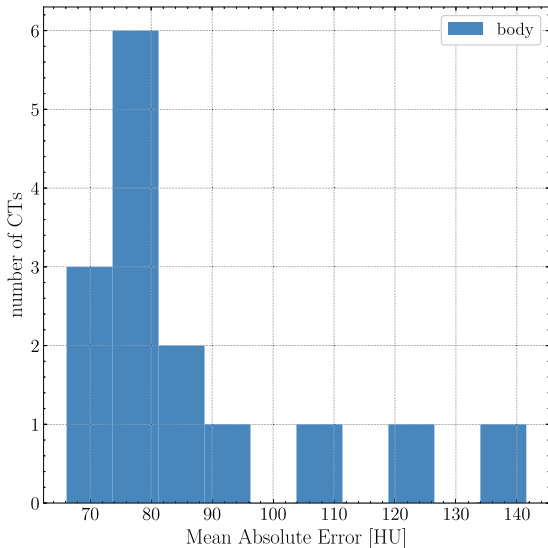


Figure 1. Histogram of the MAE computed between X-rayCT and sCT for the whole body. Three outlier can be identified with an MAE above 100 HU.

### 3 Results

The MAE between X-rayCT and sCT was  $86.9 \pm 20.2$  HU for the whole body covering the range from  $-1000$  to  $3000$  HU as depicted in the MAE histogram in Fig. 1. For

three patients especially high metric differences were observed (*i.e.* between 108 to 142 HU MAE for the body region), which were mainly caused by non-standard anatomical situations.

Evaluating all 30 plans, 30.3% of the spot displacements were caused by the mask material not possible to measure on the MRI (determined within the uncertainty interval of the peak position) as shown in Fig. 2. This peak was detected at  $0.22 \pm 0.08$  cm in beam direction.

In total 95.7% of all spot displacements were located within  $\pm 1$  cm. Besides the peak region, the spot displacements over 1 cm, ranging from  $-5.2$  to  $10.5$  cm, were evaluated with respect to a potential correlation to the distortion of the dose. Spot displacements are visualised in Fig. 2A. While the peak at  $0.22 \pm 0.08$  cm was detected in every patient, the magnitude of spot displacements varied. The number of spots with a displacement of more than 1 cm ranged from 1.3% to 5.2% between treatment plans. As an example of the most extreme cases, spot displacement histograms for patients #52 and #67 are depicted in Fig. 2B (good case) and Fig. 2C (bad case).

The sCT generation technique was able to reduce artefacts caused by metal implants observed for the teeth region in the respective patients as demonstrated in Fig. 3. Insufficient HU distributions in the sCT were observed for the representation of bones and air cavities, especially for the hyperextended head position (cf. Fig. 3). These insufficiencies led to a change of the spot positions, randomly

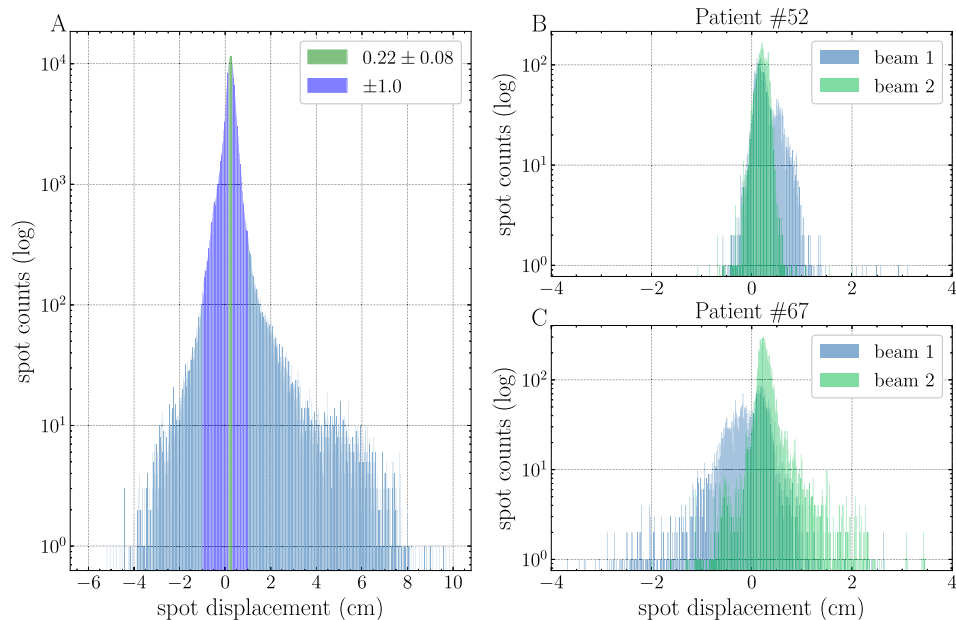


Figure 2. Histogram of the spot difference between X-rayCT and sCT computed spot positions for all treatment plans and their related spots in logarithmic scale (A). Histogram of spot differences between X-rayCT and sCT computed spot positions in logarithmic scale for patient #52 (B) and patient #67 (C).

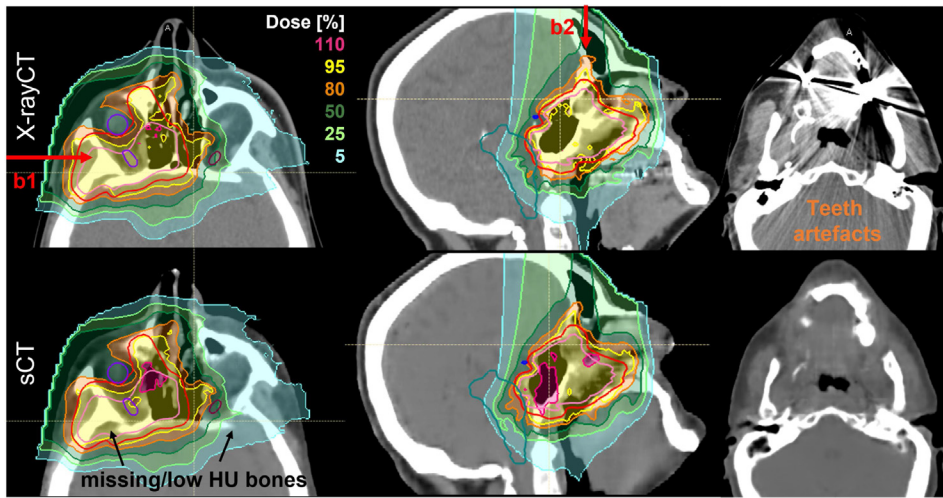


Figure 3. Representative patient (*i.e.* #67) for a hyperextended head position with a tumour located close to the surface. The patient was treated with a horizontal beam (b1) and a vertex beam (b2). The top row shows the dose distribution on the X-rayCT and the bottom row the dose distribution on the sCT. Images illustrate wrongly assigned densities on the sCT caused by the conversion method. The very right column shows teeth artefacts on the X-rayCT that are non-existing on the sCT.

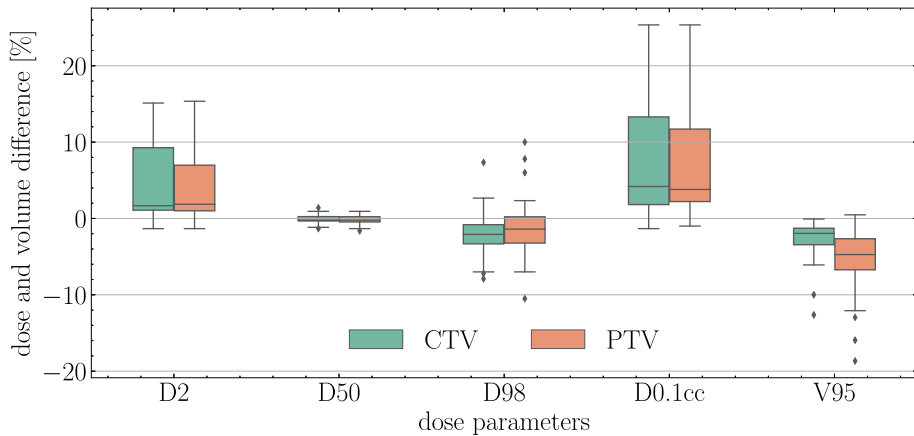


Figure 4. Differences between X-rayCT and sCT computed DVH parameters for the target structures. Dose values recomputed on the sCT were subtracted from the original dose values on the X-rayCT.

distributed over the treated area. For these cases, more than 3.4% of the spots were shifted by more than 1 cm.

For both target structures, the main dose difference was observed for the  $D_{0.1cc}$  with a median overdosage of 4.2% (−1.3 to 25.3%) for the CTV and 3.8% (−1.0 to 25.3%) for the PTV on the sCT. For the CTV  $D_{50\%}$  and  $D_2$  differed by −0.2% (−1.3 to 1.4%) and 1.7% (−1.3 to 15.1%), respectively, as summarised in Fig. 4. The median  $CI_{PTV}$  changed by 6% (1 to 26%) when recalculating the treatment plans on the sCT, while the difference for the median  $CI_{CTV}$  was only 2% (−5 to 20%). In the extreme case of #52  $CI_{PTV}$  was degraded by 10% (6 to 15%), while the  $CI_{CTV}$  changed only by 2.5% (−1 to 4%).

Three patients did not show any  $D_{2\%}$  difference larger than 5% for OARs receiving more than 5% of the prescribed dose. These were the patients for whom less than 2% of the spots were displaced by more than 1 cm. For two of those patients a low MAE was observed for body (*i.e.* between 66.1 and 79.1 HU) while the third one showed the highest value of all patients with an MAE body larger than 120 HU. Overall, no correlation between the MAE and the dosimetric parameters was found as illustrated in Fig. 5 for a patient with an MAE of 77 HU.

In 7 out of 11 patients,  $D_{2\%}$  to the optical system (chiasm or optical nerves) was deteriorated. The maximal  $D_{2\%}$  deterioration was 28.1% for the chiasm of patient #67. For the

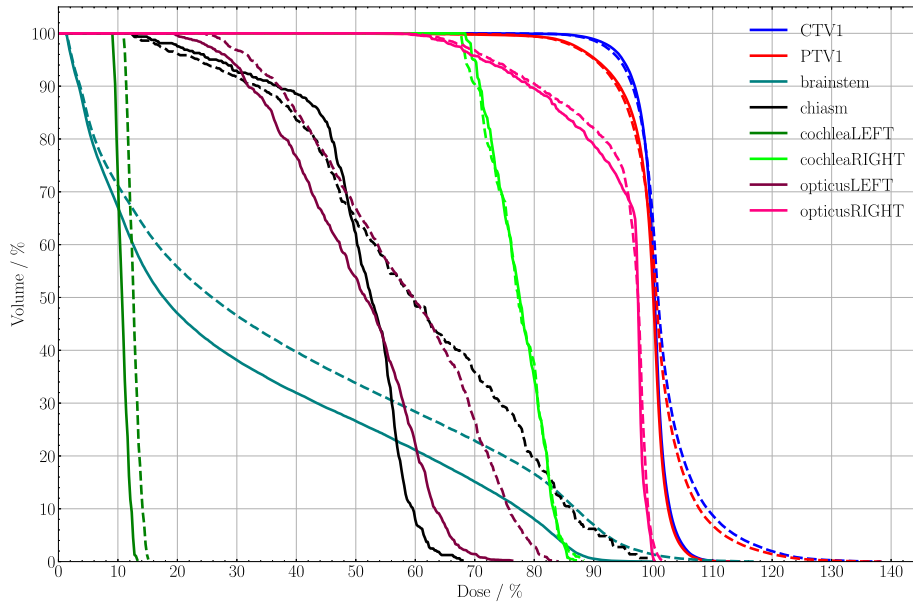


Figure 5. Patient #67: representative DVHs for CTV, PTV as well as the OARs. The solid lines represent the original dose computed on the X-rayCT, while the dashed lines show the dose recomputed on the sCT. Note that for patient #67, which was irradiated in hyperextended position, the MAE was 77 HU, which was one of the lowest MAE observed in this study.

remaining four patients, only the cochlea dose differed. Due to its small size, the cochlea was very prone to dose distortions.

As an example, the DVH of patient #67 is shown in Fig. 5 including information for OARs close to the target.

## 4 Discussion

Assuming that every radiotherapy workflow benefits from the use of sCTs, in terms of workload, resources, and imaging dose, this study focused especially on the challenges and characteristics that come along when applying carbon-ion therapy. While no commercial algorithm was validated and released for particle therapy for now, the comparable performance of recently published sCT generator algorithms (*e.g.* [32,33]) justify the use of an U-Net based algorithm. The algorithm applied in this study was trained with a proton head patient collective acquired using the same CT scanner and protocol [26]. The MAE over all 15 sCTs was  $87 \pm 20$  HU in this study while an MAE of  $65 \pm 4$  HU [32] and  $75 \pm 9$  HU [33] was reported recently by others. Overall the algorithm performed equally for carbon and proton patients with a mean difference of 4 HU. The model proved to be a good candidate for the conversion, even though some patients had major anatomical anomalies.

One uncertainty identified was the thermoplastic mask with ideal material and attenuation properties for carbon-ion treatments, which is typically used for positioning of head and neck tumour patients [34]. Along with all other

non-organic immobilisation devices the mask is not visible on MR images as the plastic material does not trigger any MR signal. Its absence influences the water equivalent thickness (WET) and therefore the beam attenuation [35,36]. While this effect is negligible for photons it has a pronounced influence on the dose distribution in particle therapy, aiming at exploiting the steep dose-fall-off to its limits. The missing mask material on the sCTs resulted in a shift of the spot positions with a mean value of  $0.22 \pm 0.08$  cm. Overriding the density of all voxels inside the patient contour with water for the X-rayCT and the sCT for two sample patients revealed a mask influence for most spots in magnitude of  $0.19 \pm 0.08$  cm, proving that the shift is a result of the mask and not affected by additional errors of the sCT conversion. A possible solution to compensate for this kind of limitation is to include a generic outline of the mask with a defined thickness in the sCT generation process, as it was done by Thummerer et al. [32] for the head support. However, the mask is stretchable and flexible and its position and size differ on a patient individual basis, so that a simple subtraction solution as for other positioning devices is not feasible. To extract the patient specific mask thickness a X-rayCT is required which is limited to a workflow that uses sCTs as control images during treatment and not to replace the X-rayCT.

A major challenge for particle treatments in the head and neck area are the sinonasal cavities, with their ability to change the filling status according to clinical situation (air, fluid, solid tissue) [37]. By a variation of the filling status

of these cavities during treatment, a spot position can be easily displaced by several millimeters causing a substantial alteration in the dose distribution. Within this study, MRI and X-rayCT were acquired within one hour and thus guaranteed the same filling status and anatomy in the tumour region, resulting in well presented air cavities on the sCT for anatomical standard situations. For unique patient immobilisations or special anatomical situations, however, air cavities could not always be maintained in the MRI to sCT conversion process. In those cases a larger training dataset could improve the results as the discrepancies are not caused by anatomical changes between the imaging modalities.

While the weaker performance of the sCT model caused by a challenging immobilisation, like hyperextension of the head, can theoretically be compensated by increasing the number of training datasets, some anatomical conditions (*e.g.* after surgery) remain unique and thus a source of uncertainty. Such unique cases, however, are common in carbon-ion therapy. It was shown in this study that recalculating the dose on the sCT had a smaller effect on  $CI_{CTV}$  than on  $CI_{PTV}$ , as described in the results. Thus, the PTV margin compensated well for spot uncertainties caused by the missing mask material, patient mispositioning and anomalies in the nasal cavity regions, revealing that the observed differences are in the same magnitude as observed for setup uncertainties [38]. However, in general, no correlation was found between the spot displacement and the CI. Especially for large targets even a pronounced random shift of spot positions did not necessarily result in unsatisfying target coverage, just in a re-arrangement of cold and hot spots within the target area.

The degree of dose deterioration for the OARs strongly depended on the position of the OARs in relation to the PTV as well as the presence of air cavities and bones in the beam path. A generalisation of the dose changes for the OAR proved to be challenging and resulted in differences up to 28%. Published data never revealed such large changes of dose parameters for proton therapy when recalculating treatment plans on sCTs. There averaging of dose values was possible for the included patient collective revealing the most extreme outliers for dose deterioration with 10% relative dose [32]. For each individual patient the source of dose distortion in an OAR was related to anatomical differences between the X-rayCT and MRI, such as a change of the patient surface or an incorrect representation of bones or air cavities and their respective density values, underlining the relevance of the previously mentioned challenges.

The wrong assignment of density values for certain body components on the sCT, especially for bones, could be addressed by a dedicated sCT electron density to stopping power calibration curve [29] for a more accurate dose calculation. This step would require additional sophisticated measurements for creating and validating an sCT conversion

curve, which goes beyond the frame of this study. However, also the X-rayCT, for which the applied conversion curve was validated, is associated with an inherent uncertainty of up to 3% that comes along with the conversion from HU to stopping power [39]. Stopping power and range prediction in particle therapy is known to be a large source of uncertainty, which could be potentially improved on the basis of dual energy CT (DECT) data [40,41,39]. However, this requires a complete training set including MRI sequences and DECT information of patients.

Even when it seems to be a long way towards a full MR-only workflow in carbon-ion therapy, the use of sCTs in certain steps of the workflow has a high potential. Recent investigations on the performance of sCTs in a proton therapy workflow compared to photons showed promising results [11,42]. As demonstrated in this study, sCTs, in addition to the X-rayCTs, can reduce uncertainties caused by metal implants, which highly disturb the dose distributions for carbon-ion patients. Furthermore, the use of MRI-based sCTs reduces the error propagated from the rigid registration of MRI and CT when transferring structures between those image modalities.

Compared to existing literature [32,33] the MAE of  $87 \pm 20$  HU should be sufficient to serve as the basis for an accurate dose re-calculation in photon and proton therapy. The presented results for carbon-ion therapy, especially on the dose differences for OARs and spot displacement demonstrated the necessity for an improved training data set for the application of sCTs based on MRI. To bring sCTs closer to clinical routine in carbon-ion therapy the training dataset has to be enlarged including as many special cases as possible, which is not trivial for a single carbon-ion center. A possible approach is to collect data from various centres or, on a long run, to extend the training dataset by artificial images, as proposed by Fetty et al. [43]. However, a multicentre approach brings along new challenges, as every carbon-ion therapy centre uses different image protocols and different MRI scanners. Thus a sequence and scanner independent algorithm is required. The sCT generator used in this study offers the possibility to extend the training dataset with data from multiple institutes independent of the scanner or the sequences used, which would not be possible with a vendor specific solution, which usually requires sCT-specific sequence not tailored for diagnostic purposes. The use of clinical MR sequences will open new possibilities for multicentric data collection for training purposes and will not add any additional burden to the patient [26].

## 5 Conclusion

The use of sCTs in a carbon-ion treatment workflow has a high potential but comes along with challenges unknown from advanced photon and proton therapy. Unique patients

anatomy and immobilisation strategies can result in a reduced sCT image quality and a high uncertainty in HU assignment to bones and air cavities. Individualised beam configurations and highly modulated treatment plans challenge the beam attenuation calculation and may result in erroneous OAR dose predictions on the sCT. The deterioration of the carbon-ion beam by the patient individual mask material, which is not visible on the MR, needs to be overcome for the use of sCTs in the clinical carbon-ion workflow.

### Declaration of Competing Interest

The authors declare that they have no known competing financial interests or personal relationships that could have appeared to influence the work reported in this paper.

### Acknowledgments

The research was partially funded by the Austrian Science Fund (FWF) (project number: P30065-B27), the Austrian Research Promotion Agency (FFG, project number 867619), and the European Union (EUROSTARS-2 CoD9: 12326 ILLUMINUS) and the Gesellschaft für Forschungsförderung Niederösterreich GmbH and the state government of Lower Austria.

### References

- [1] Li Y, Kubota Y, Tashiro M, Ohno T. Value of three-dimensional imaging systems for image-guided carbon ion radiotherapy. *Cancers* 2019;11(3). <https://doi.org/10.3390/cancers11030297>.
- [2] van der Heide UA, Frantzen-Steneker M, Astrinidou E, Nowee ME, van Houdt PJ. MRI basics for radiation oncologists. *Clin Translat Radiat Oncol* 2019;18:74–79. <https://doi.org/10.1016/j.ctro.2019.04.008>.
- [3] Zimmermann L, Buschmann M, Herrmann H, Heilemann G, Kuess P, Goldner G, et al. An MR-only acquisition and artificial intelligence based image-processing protocol for photon and proton therapy using a low field MR. *Z Med Phys* 2021;31(1):78–88. <https://doi.org/10.1016/j.zemedi.2020.10.004>.
- [4] Murray J, Tree AC. Prostate cancer – Advantages and disadvantages of MR-guided RT. *Clin Translat Radiat Oncol* 2019;18:68–73. <https://doi.org/10.1016/j.ctro.2019.03.006>.
- [5] de Muinck Keizer DM, van der Voort van Zyp JRN, de Groot-van Breugel EN, Raaymakers BW, Lagendijk JJW, de Boer HCJ. On-line daily plan optimization combined with a virtual couch shift procedure to address intrafraction motion in prostate magnetic resonance guided radiotherapy. *Phys Imaging Radiat Oncol* 2021;19:90–95. <https://doi.org/10.1016/j.phro.2021.07.010>.
- [6] Palmér E, Karlsson A, Nordström F, Petruson K, Siversson C, Ljungberg M, et al. Synthetic computed tomography data allows for accurate absorbed dose calculations in a magnetic resonance imaging only workflow for head and neck radiotherapy. *Phys Imaging Radiat Oncol* 2021;17:36–42. <https://doi.org/10.1016/j.phro.2020.12.007>.
- [7] MacKay RI. Image guidance for proton therapy. *Clin Oncol* 2018;30(5):293–298. <https://doi.org/10.1016/j.clon.2018.02.004>.
- [8] Hoffmann A, Oborn B, Moteabbed M, Yan S, Bortfeld T, Knopf A, et al. Mr-guided proton therapy: a review and a preview. *Radiat Oncol* 2020;15:129. <https://doi.org/10.1186/s13014-020-01571-x>.
- [9] Oborn BM, Dowdell S, Metcalfe PE, Crozier S, Mohan R, Keall PJ. Future of medical physics: Real-time MRI-guided proton therapy. *Med Phys* 2017;44. <https://doi.org/10.1002/mp.12371>.
- [10] Padilla-Cabal F, Resch AF, Georg D, Fuchs H. Implementation of a dose calculation algorithm based on Monte Carlo simulations for treatment planning towards mri guided ion beam therapy. *Physica Med* 2020;74:155–165. <https://doi.org/10.1016/j.ejmp.2020.04.027>.
- [11] Maspero M, Bentvelzen LG, Savenije MHF, Guerreiro F, Seravalli E, Janssens GO, et al. Deep learning-based synthetic CT generation for paediatric brain MR-only photon and proton radiotherapy. *Radiother Oncol* 2020;153:197–204. <https://doi.org/10.1016/j.radonc.2020.09.029>.
- [12] Neppi S, Landry G, Kurz C, Hansen DC, Hoyle B, Stöcklein S, et al. Evaluation of proton and photon dose distributions recalculated on 2D and 3D Unet-generated pseudoCTs from T1-weighted MR head scans. *Acta Oncol* 2019;58(10):1429–1434. <https://doi.org/10.1080/0284186X.2019.1630754>, ISSN 1651226X.
- [13] Shafai-Erfani G, Lei Y, Liu Y, Wang Y, Wang T, Zhong J, et al. MRI-based proton treatment planning for base of skull tumors. *Int J Particle Therapy* 2020;6(2):12–25. <https://doi.org/10.14338/IJPT-19-0062.1>, ISSN 23315180.
- [14] Fossati P, Perpar A, Stock M, Georg P, Carlino A, Gora J, et al. Carbon Ion Dose Constraints in the Head and Neck and Skull Base: Review of MedAustron Institutional Protocols. *Int J Particle Therapy* 2021;8:25–35. <https://doi.org/10.14338/IJPT-20-00093.1>.
- [15] Malouff TD, Mahajan A, Krishnan S, Beltran C, Seneviratne DS, Trifiletti DM. Carbon Ion Therapy: A Modern Review of an Emerging Technology. *Front Oncol* 2020;10. <https://doi.org/10.3389/fonc.2020.00082>.
- [16] Koto M, Hasegawa A, Takagi R, Fujikawa A, Morikawa T, Kishimoto R, et al. Risk factors for brain injury after carbon ion radiotherapy for skull base tumors. *Radiother Oncol* 2014;111(1):25–29. <https://doi.org/10.1016/j.radonc.2013.11.005>.
- [17] Gillmann C, Lomax AJ, Weber DC, Jäkel O, Karger CP. Dose-response curves for MRI-detected radiation-induced temporal lobe reactions in patients after proton and carbon ion therapy: Does the same RBE-weighted dose lead to the same biological effect? *Radiother Oncol* 2018;128(1):109–114. <https://doi.org/10.1016/j.radonc.2018.01.018>.
- [18] Bhattacharyya T, Koto M, Ikawa H, Hayashi K, Hagiwara Y, Makishima H, et al. First prospective feasibility study of carbon-ion radiotherapy using compact superconducting rotating gantry. *Brit J Radiol* 2019;92(1103):20190370. <https://doi.org/10.1259/bjr.20190370>.
- [19] Iwata Y, Noda K, Murakami T, Shirai T, Furukawa T, Fujita T, et al. Development of a superconducting rotating-gantry for heavy-ion therapy. *Nucl Instrum Methods Phys Res Sect B* 2013;317:793–797. <https://doi.org/10.1016/j.nimb.2013.03.050>.
- [20] Fuchs R, Weinrich U, Sust E. Assembly of the carbon beam gantry at the heidelberg ion therapy (HIT) accelerator. EPAC08 2008.
- [21] Kleffner C, Weinrich U. Commissioning of the carbon beam gantry at the heidelberg ion therapy (HIT) accelerator. EPAC08 2008.
- [22] Siversson C, Nordström F, Nilsson T, Nyholm T, Jonsson J, Gunnlaugsson A, et al. Technical Note: MRI only prostate radiotherapy planning using the statistical decomposition algorithm. *Med Phys* 2015;42:6090–6097. <https://doi.org/10.1118/1.4931417>.
- [23] Persson E, Gustafsson C, Nordström F, Sohlin M, Gunnlaugsson A, Petruson K, et al. MR-OPERA: A Multicenter/Multivendor Validation of Magnetic Resonance Imaging-Only Prostate Treatment Planning Using Synthetic Computed Tomography

- Images. *Int J Radiat Oncol Biol Phys* 2017;99:692–700. <https://doi.org/10.1016/j.ijrobp.2017.06.006>.
- [24] Spadea MF, Maspero M, Zaffino P, Seco J. Deep learning based synthetic-ct generation in radiotherapy and pet: A review. *Med Phys* 2021. <https://doi.org/10.1002/mp.15150>.
  - [25] Kazemifar S, McGuire S, Timmerman R, Wardak Z, Nguyen D, Park Y, et al. MRI-only brain radiotherapy: Assessing the dosimetric accuracy of synthetic CT images generated using a deep learning approach. *Radiat Oncol* 2019;136:56–63. <https://doi.org/10.1016/j.radonc.2019.03.026>.
  - [26] Zimmermann L, Knäusl B, Stock M, Lütgendorf-Caucig C, Georg D, Kuess P. Using an MRI sequence independent convolutional neural network for synthetic head ct generation in proton therapy. *Z Med Phys* 2022;32(2):218–227. <https://doi.org/10.1016/j.zemedi.2021.10.003>.
  - [27] Stock M, Georg D, Ableitinger A, Zechner A, Utz A, Mumot M, et al. The technological basis for adaptive ion beam therapy at MedAustron: Status and outlook. *Z Med Phys* 2018;28(3):196–210. <https://doi.org/10.1016/j.zemedi.2017.09.007>, ISSN 09393889.
  - [28] Elsässer T, Krämer M, Scholz M. Accuracy of the local effect model for the prediction of biologic effects of carbon ion beams in vitro and in vivo. *Int J Radiat Oncol Biol Phys* 2008;71(3):866–872. <https://doi.org/10.1016/j.ijrobp.2008.02.037>.
  - [29] Schneider U, Pedroni E, Lomax A. The calibration of CT hounsfield units for radiotherapy treatment planning. *Phys Med Biol* 1996;41(1):111–124. <https://doi.org/10.1088/0031-9155/41/1/009>.
  - [30] Paddick I. A simple scoring ratio to index the conformity of radiosurgical treatment plans. *J Neurosurg* 2000;93(Suppl 3):219–222.
  - [31] The International Commission on Radiation Units and Measurements. ICRU Report 91 - Prescribing, Recording, and Reporting of Stereotactic Treatments with Small Photon Beams; 2014.
  - [32] Thummerer A, de Jong BA, Zaffino P, Meijers A, Marmitt GG, Seco J, et al. Comparison of the suitability of CBCT- and MR-based synthetic CTs for daily adaptive proton therapy in head and neck patients. *Phys Med Biol* 2020;65(23):235036. <https://doi.org/10.1088/1361-6560/abb1d6>.
  - [33] Dinkla AM, Florkow MC, Maspero M, Savenije MHF, Zijlstra F, Doornaert PAH, et al. Dosimetric evaluation of synthetic CT for head and neck radiotherapy generated by a patch-based three-dimensional convolutional neural network. *Med Phys* 2019;46(9):4095–4104. <https://doi.org/10.1002/mp.13663>.
  - [34] Zechner A, Ziegler I, Hug E, Lütgendorf-Caucig C, Stock M. Evaluation of the inter- and intrafraction displacement for head patients treated at the particle therapy centre medaustron based on the comparison of different commercial immobilisation devices. *Z Med Phys* 2021. <https://doi.org/10.1016/j.zemedi.2021.01.007>.
  - [35] Fellin F, Righetto R, Fava G, Trevisan D, Amelio D, Farace P. Water equivalent thickness of immobilization devices in proton therapy planning – Modelling at treatment planning and validation by measurements with a multi-layer ionization chamber. *Physica Med* 2017;35:31–38. <https://doi.org/10.1016/j.ejmp.2017.02.010>.
  - [36] Olch AJ, Gerig L, Li H, Mihaylov I, Morgan A. Dosimetric effects caused by couch tops and immobilization devices: Report of aapm task group 176. *Med Phys* 2014;41:061501. <https://doi.org/10.1111/14876299>.
  - [37] Placidi L, Bolsi A, Lomax AJ, Schneider RA, Malyapa R, Weber DC, et al. Effect of Anatomic Changes on Pencil Beam Scanned Proton Dose Distributions for Cranial and Extracranial Tumors. *Int J Radiat Oncol Biol Phys* 2017;97(3):616–623. <https://doi.org/10.1016/j.ijrobp.2016.11.013>.
  - [38] Kanai T, Furuchi W, Mori S. Evaluation of patient positional reproducibility on the treatment couch and its impact on dose distribution using rotating gantry system in scanned carbon-ion beam therapy. *Physica Med* 2019;57:160–168. <https://doi.org/10.1016/j.ejmp.2018.12.013>.
  - [39] Peters N, Wohlfahrt P, Dahlgren CV, de Marzi L, Ellerbrock M, Fracciolla F, et al. Experimental assessment of inter-centre variation in stopping-power and range prediction in particle therapy. *Radiother Oncol* 2021;163:7–13. <https://doi.org/10.1016/j.radonc.2021.07.019>.
  - [40] Liu R, Lei Y, Wang T, Zhou J, Roper J, Lin L, et al. Synthetic dual-energy CT for MRI-only based proton therapy treatment planning using label-GAN. *Phys Med Biol* 2021;66(6):65014. <https://doi.org/10.1088/1361-6560/abe736>.
  - [41] Van Elmpt W, Landry G, Das M, Verhaegen F. Dual energy CT in radiotherapy: Current applications and future outlook. *Radiother Oncol* 2016;119(1):137–144. <https://doi.org/10.1016/j.radonc.2016.02.026>.
  - [42] Depauw N, Keyriläinen J, Suilamo S, Warner L, Bzdusek K, Olsen C, et al. MRI-based IMPT planning for prostate cancer. *Radiother Oncol* 2020;144:79–85. <https://doi.org/10.1016/j.radonc.2019.10.010>.
  - [43] Fetty L, Bylund M, Kuess P, Heilemann G, Nyholm T, Georg D, et al. Latent Space Manipulation for High-Resolution Medical Image Synthesis via the StyleGAN. *Z Med Phys* 2020. <https://doi.org/10.1016/j.zemedi.2020.05.001>.

Available online at: [www.sciencedirect.com](http://www.sciencedirect.com)

ScienceDirect